Magneto-dielectric effect in relaxor superparaelectric Tb_2CoMnO_6 film

R. Mandal,[1,2,*] M. Chandra,[3] V. Roddatis,[4] P. Ksoll,[2] M. Tripathi,[3] R. Rawat,[3] R. J. Choudhary,[3] and V. Moshnyaga[2,†]

[1]*Department of Physics, Indian Institute of Science Education and Research, Pune 411008, India*

[2]*Erstes Physikalisches Institut, Georg-August-Universität Göttingen, Friedrich-Hund-Platz 1, 37077 Göttingen, Germany*

[3]*UGC-DAE Consortium for Scientific Research, Indore Centre, University Campus, Khandwa Road, Indore 452017, India*

[4]*Institut für Materialphysik, Georg-August-Universität Göttingen, Friedrich-Hund-Platz 1, 37077 Göttingen, Germany*

(Received 17 October 2019; revised manuscript received 23 January 2020; accepted 2 March 2020; published 19 March 2020; corrected 28 August 2020)

We report magneto-dielectric properties of partially B-site ordered monoclinic Tb_2CoMnO_6 double perovskite thin film epitaxially grown on $Nb:SrTiO_3(100)$ substrates by metalorganic aerosol deposition technique. Transmission electron microscopy and electron energy loss spectroscopy mapping shows the presence and distribution of both Co^{2+} and Co^{3+} ions in the film, evidencing a partial *B*-site disorder, which was further confirmed by the observation of reduced saturation magnetization at low temperatures. The ferromagnetic Curie temperature, $T_C = 110\,\mathrm{K}$, is slightly higher as compared to the bulk value (100 K) probably due to an in plane epitaxy tensile strain. Temperature dependent dielectric study reveals an unexpected high temperature dipolar relaxor-glass-like transition at a temperature $T^* \sim 190\,\mathrm{K} > T_C$, which depends on the applied frequency and indicates a superparaelectric behavior. Two different dielectric relaxation peaks have been observed; they merge at T^* where likely a coupling to the disorder-induced short range charge-spin correlations results in a 4% magneto-dielectric coupling.

DOI: 10.1103/PhysRevB.101.094426

I. INTRODUCTION

Magneto-dielectrics and magneto-electric materials with the coupled magnetic and electric dipolar order parameters are of fundamental as well as of technological importance. Rare-earth-based perovskite oxides have been proved to be potential candidates for the next generation memory and spintronic device applications [1–7]. $A_2BB'O_6$ (*A* is a rare earth cation, *B* and *B'* are transition metal ions) double perovskites with the layered $ABO_3/AB'O_3$ cation-ordered structure along the [111] axis represent themselves an emerging and promising platform to study strong electronic correlations, complex magnetic structure, spin-lattice interaction, and magneto-dielectric coupling [8,9].

$R_2(Co/Ni)MnO_6$ (where $R =$ La to Lu) system having a monoclinic structure with $P2_1/n$ space group is especially attractive as they possess an insulating ferromagnetic (FMI) behavior with relatively high Curie temperatures, $T_C \sim$ 200–300 K, allowing a high temperature magneto-dielectric coupling. FMI originates from a 180°- superexchange interaction between high spin Co^{2+}/Ni^{2+} and Mn^{4+} ions, described by the second Goodenough-Kanamori-Anderson rule [10–12]. The FM ordering as well as dielectric behavior depend strongly on the B-site ordering which controls the superexchange interaction along with hoping of charge. The fully and partially B-site ordered La_2CoMnO_6 has been well explored due to a reasonably high ferromagnetic Curie temperature, $T_C = 230\,\mathrm{K}$ [13], spin-phonon coupling [11]; they reveal a weak magneto-dielectric effect (3%) [14]. Partially disordered La_2NiMnO_6 has been viewed as a promising multiglass material where two different glassy states (spin and dipolar) were observed simultaneously, resulting in a stronger magneto-dielectric coupling constant ($\epsilon_{MD} = \frac{\epsilon'(8T)-\epsilon'(0T)}{\epsilon'(0T)} \times 100$) $\sim 16\%$ at room temperature [15]. Considering the smaller radii rare-earth ions in the *A*-site ($R =$ Pr to Lu) the ferromagnetic T_C decreases considerably (down to $T_C = 48\,\mathrm{K}$ for Lu) [8] along with spin-phonon interaction [16]. The trend in the dielectric behavior also remains unchanged from bigger to smaller *A*-site cations as found in bulk $(La/Tb/Y)_2CoMnO_6$ where dielectric constant decreases monotonically with lowering temperature [17]. The La_2CoMnO_6 (LCMO) from the concerned rare earth double perovskite family has been reported to possess a large dielectric constant at room temperature, which gradually decreases with lowering the temperature [17]. Taking ions with smaller ionic radii, like Y^{3+} and Tb^{3+} in the *A*-site, the trend of decreasing dielectric constant monotonically towards lowering temperature remains similar with no significant deviation [18]. The overall behavior is the same in the case of epitaxial LCMO thin films though the dielectric constant becomes very low [14]. A controllable disorder in a perovskite or double perovskite system can create a dipolar glass that can couple with its magnetic subsystem, inducing a novel magneto-dielectric or rare multiglass behavior [19]. Tb^{3+} with a small cation radius in the A-site has a special significance as it can tune and stabilize a different hexagonal structure in a strained thin film, which cannot sustain in the bulk form as observed in $TbMnO_3$ [20]. With all these experimental observations and intuitions, the Tb-based double perovskite thin films with controllable B-site (partial) ordering could be suggested as an important and exclusive playground for studying magnetic and dielectric transitions along with possible coupling between them.

*rajesh.mandal@students.iiserpune.ac.in

†vmosnea@gwdg.de

Here we report the epitaxial growth of monoclinic Tb_2CoMnO_6/Nb : $SrTiO_3$(100) thin film by using a metalorganic aerosol deposition (MAD) technique [21]. The established partial B-site disorder in the film is accompanied by an unexpected high temperature relaxor glassy transition along with a superparaelectric behavior. The asymmetrical nature of the temperature dependent dielectric constant is manifested with the three different polarized nanoregions (PNR) present in the system. Moreover, two different dielectric relaxation peaks in frequency domain along with a 4% magneto-dielectric coupling was observed probably due to the interaction of the B-site-disorder-induced local spin moments with the PNRs.

II. EXPERIMENTAL SECTION

Tb_2CoMnO_6 (TCMO) films have been grown by a metalorganic aerosol deposition technique on commercial electrically conducting 0.5% Nb-doped $SrTiO_3$(100) substrates (Crystal GmbH). Acetylacetonates of Tb, Mn, and Co were used as precursors. Precursor solutions in dimethylformamide with concentration 0.02 M (for both Co and Mn precursor) and empirically found molar ratio $Tb/(Co + Mn) = 1.1$ were prepared. The films with thickness, $d = 80$ nm, were grown by spraying the precursor solution by using dry compressed air onto a substrate heated to $T_{sub} \sim 900\,^{\circ}C$. The films were grown with an average growth rate of $v = 15$ nm/min and were cooled down to room temperature in 20 min after deposition. X-ray diffraction (XRD) characterization was performed by using the "Bruker D8" spectrometer with Cu $K_{\alpha 1,2}$ radiation in a Θ-2Θ Bragg-Brentano geometry. Magnetization as a function of temperature and magnetic field, applied parallel to the film surface, was measured using commercial 7T-superconducting quantum interference device-vibrating-sample magnetometer (Quantum Design Inc., USA) system. Magnetization vs temperature was measured following the conventional protocols of zerofield-cooled warming (ZFC) and field-cooled warming (FCW) cycles in an applied magnetic field $H = 100$ Oe. The local structure of TCMO films was studied by scanning transmission electron microscopy and electron energy loss spectroscopy (EELS) using a FEI Titan 80–300 G2 environmental transmission electron microscope (TEM), operated at an acceleration voltage of 300 kV. The TEM is equipped with a Gatan Imaging Filter Quantum 965 ER. EELS spectra were taken with a dispersion of 0.05 eV/channel. The convergence and collection semiangles were about 10 and 22 mrad, respectively. TEM lamellas were prepared by a focused ion beam lift-out technique using a Thermo-Fischer (former FEI) Helios 4UC instrument. The temperature- and magnetic-field-dependent complex dielectric measurements were performed using a homemade insert coupled with 9-T superconducting magnet and a Keysight E4980A LCR-meter operating at frequency range $f = 20$ Hz–2 MHz.

III. RESULTS AND DISCUSSION

Temperature dependence of the ZFC and FC magnetic susceptibility, $\chi(T)$, of the TCMO film, measured for $\mu_0 H = 100$ Oe, is shown in Fig. 1(a). One can see a phase

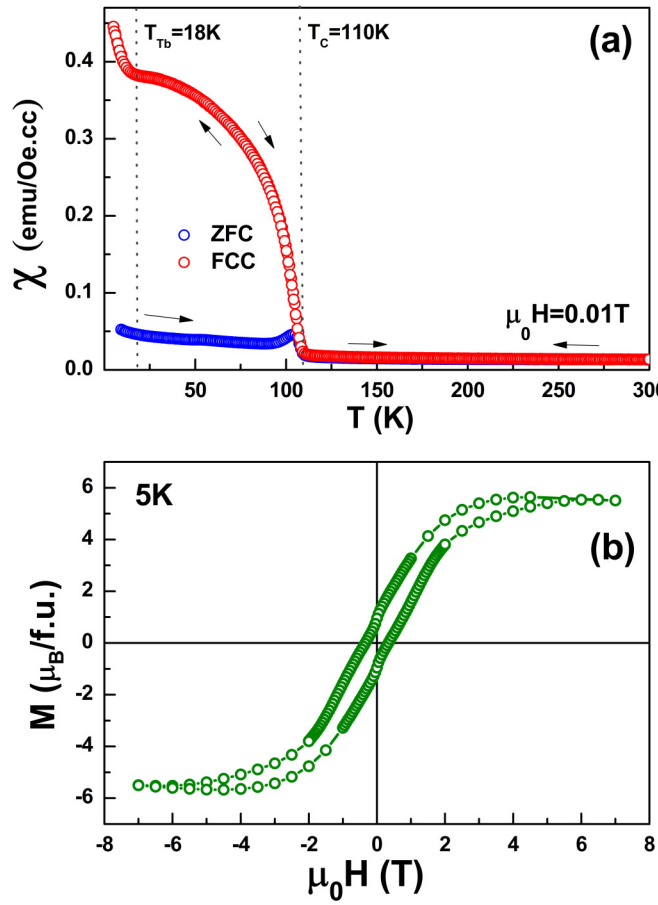

FIG. 1. (a) Zero- (blue, ZFC) and field-cooled (red, FC) magnetic susceptibility [$\chi(T)$] as a function of temperature (T) in the TCMO film; (b) Isothermal magnetization with applied external magnetic field at 5 K.

transition at $T_C = 110$ K, below which the long range ferromagnetic ordering develops due the superexchange interaction between Co^{2+} and Mn^{4+} ions [12]. The transition seems to be of a second order as it is not apparently sharp and no warming/cooling hysteresis was observed. The transition temperature in our TCMO film is a bit higher than that observed in a Tb_2CoMnO_6 single crystal (100 K) [22], likely due to an in-plane epitaxial tensile strain in the TCMO thin film, $\varepsilon = -0.6\%$, evaluated from the XRD pattern [23] (see Fig. SM-1), which shows an out-of-plane epitaxy. The bifurcation between ZFC and FC curves denotes the magnetic irreversibility in the system due to the presence of antiferromagnetic/FM competing interactions among magnetic domains, which are characteristic for ferro- and ferrimagnetic systems with large coercivity in the ordered phase, irrespective of what origin. It means that along with the dominating Co^{2+}/Mn^{4+} FM superexchange the AFM interactions of Mn^{4+}/Mn^{4+} and/or Co^{2+}/Co^{2+} type could be present, although no additional features were observed at low temperatures due to the domain-wall depinning process similar to that observed in a single crystal [22]. The anomalous increase in FC curve at 18 K is due to the ordering of spins of Tb^{3+} ions, which are likely FM coupled to the Co^{2+}/Mn^{4+} sites. In Fig. 1(b) the field dependence of the isothermal magnetization, $M(H)$,

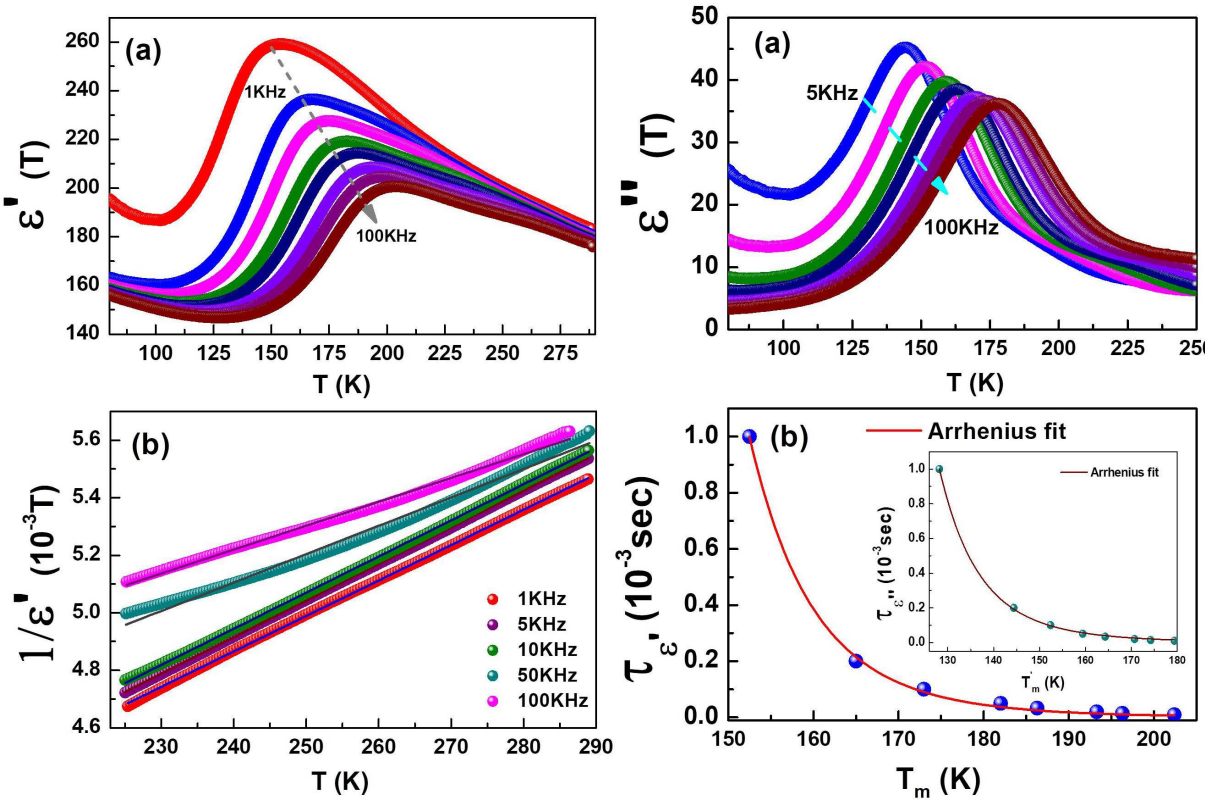

FIG. 2. (a) Dielectric constant $[\epsilon'(T)]$ vs temperature with different applied frequencies (1–100 KHz); (b) Curie-Weiss fit for the $\epsilon'(T)$ above the relaxor glass transition for different frequencies; (c) Temperature dependence of the dielectric loss part $\epsilon''(T)$ with different applied frequencies showing relaxation peaks; (d) Arrhenius fit for the relaxation time vs peak temperature for the dielectric constant $\epsilon'(T)$ and dielectric loss $\epsilon''(T)$ (inset).

measured at 5 K is shown. The evaluated magnetization close to saturation, $M_S \sim 5.5\,\mu_B$/f.u., is significantly smaller than the theoretical value ($6\,\mu_B$/f.u.) for a fully B-site ordered Co^{2+}/Mn^{4+} system. Moreover, the Tb^{+3} ions possess an even higher moment of $9.72\,\mu_B/Tb^{3+}$ due to the spin-orbit coupling and, considering their additive contribution, the total magnetic moment of the TCMO system should be even much larger. Recently, the TCMO single crystal has been shown to have a strong magnetic anisotropy of Tb^{3+} ions, which prefers to order along the c axis yielding a large value of $M_S \sim 9.73\,\mu_B$/f.u. [22]. As for our TCMO/Nb:STO(001) film the c axis according to XRD [23] (see Fig. SM-1) stays perpendicular to the film plane, and the observed value of $M_S \sim 5.5\,\mu_B$/f.u. seems to be quite small though we do not know the exact orientation of the magnetic easy axis for our film. From the trend and comparison to the single crystal data it could be concluded that the direction of applied magnetic field is somewhere in between the magnetic easy and hard axis of the film. A very small value of remnant $M_r = 1.1\,\mu_B$/f.u. and a large coercive field of $H_C = 0.35$ T as compared to that of the TCMO single crystal is in line with significant amount of Mn^{3+} disorder along with Co^{2+}-O-Co^{2+} and Mn^{4+}-O-Mn^{4+} interactions, contributing to the AFM phase boundaries and developing FM/AFM competitive interactions [12]. The presence of Mn^{3+}/Co^{3+} ions, making a finely distributed partial disorder at nm scale within the film, as well as a dominance of Co^{2+}/Mn^{4+} oxidation states responsible for the main FM phase has been further confirmed by EELS mapping in high-resolution TEM [24], shown in Fig. SM-2.

In Fig. 2(a) we present the temperature dependence of the real part of dielectric constant, $\epsilon'(T)$, measured for different frequencies, showing a broad maxima of $\epsilon'(T)$, which is of the same order as that observed in the LCMO film [14]. The temperature of the maximum, T_m, depends on the frequency and shifts to higher temperatures with increasing frequency. This kind of glassy behavior is very new for the A_2CoMnO_6 double perovskites and probably indicates a ferroelectric relaxor behavior, which is not associated with any structural transition in the system. With further lowering the temperature ($T \leqslant 100$–120 K) the $\epsilon'(T)$ starts to increase again possibly due to the electronic contribution from the conducting Nb:STO substrate and the substrate/film interface.

The observed ferroelectric relaxor behavior can be fitted with the Curie-Weiss law, $\epsilon' = C/(T - \theta)$ in the paraelectric region [25] above the frequency dependent relaxor transition temperature, $T_m \approx 150$–200 K, as shown in Fig. 2(b). The fitting parameters are presented in Table SM-1 [26]. At low frequencies the data were fitted well with the Curie constant, $C = 8 \times 10^3$, and the Curie temperature, $\theta \sim 150$ K, respectively. With increasing frequency, the data start to deviate from the Curie-Weiss law. As for high frequencies the transition temperatures, T_m, increase, the fitting range becomes to be not far away from the transition temperature. The short range correlations among electric dipoles emerge, being frequency dependent and causing deviation from an ideal ferroelectric

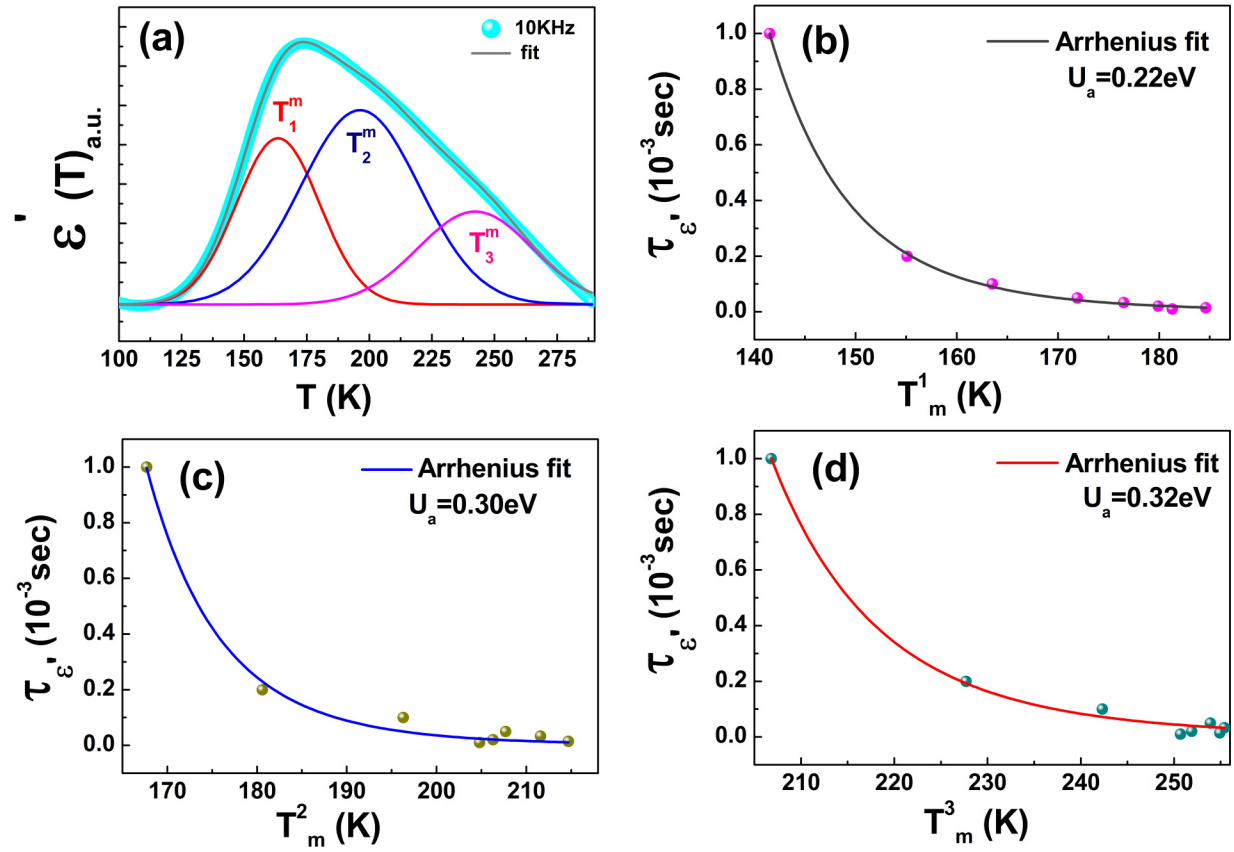

FIG. 3. (a) Gaussian fit for the temperature dependent dielectric constant $\epsilon'(T)$ and deconvolution of three peaks signifying the presence of three different types of PNRs; (b), (c) and (d) are Arrhenius fits for three relaxation times related to these three different peak temperatures: T_m^1, T_m^2 and T_m^3, respectively.

behavior. The plausible interpretation is the formation of small Polar Nano Regions (PNR), having different responses for sufficiently high frequency. For an ideal ferroelectric case the Curie-Weiss fit should not depend on the applied frequency.

In Fig. 2(c) one can see a broad relaxation peak (T_m) in the temperature dependence of the dielectric loss, $\epsilon''(T)$, which also shows a frequency dispersion. The observed relaxation in both real, $\epsilon'(T)$, and imaginary part, $\epsilon''(T)$, of dielectric constant could be interpreted in the framework of a dipolar glass model [27]. It considers small dipolar regions, induced in the system by the *B*-site disorder, the dipole moment of which fluctuates/vibrates thermally at high temperatures $T > T_m$. Analogously to the spin glass, the dipoles are expected to be frozen at low temperatures. The freezing temperature (T_f) is finite if the interaction between dipoles is strong enough. The dynamics of a PNR can be described by the so called Vogel-Fulcher (VF) formalism $f^{-1} = \tau_0 \exp[U_a/K_B(T_m - T_f)]$, where f is the frequency of an applied electric field, and T_m is the relaxation peak maxima [28–31]. If the electrostatic interaction among the dipoles is not strong enough to freeze them cooperatively, then dipoles can vibrate with external ac electric field at any finite temperature and can show a thermally activated Arrhenius behavior down to $T_f \rightarrow 0$ K. Both VF and the Arrhenius law $f^{-1} = \tau_0 \exp[U_a/K_B(T_m)]$ as well as a power law were tried to fit the data. The best fit was obtained with Arrhenius behavior, shown in Fig. 2(d) for both ϵ and ϵ. The activation energies, calculated from the fits are $U_a = 0.25$ eV and 0.16 eV for ϵ and ϵ, respectively; they look physically reasonable and are of the same order of magnitude as activation energies ~0.1 eV for a typical relaxor ferroelectric [26]. The evaluated relaxation time, $\tau_0 = 1.59 \times 10^{-12}$ s, corresponds roughly to characteristic phonon frequencies of few THz, obtained from Raman spectra of similar double perovskites films [11].

The observed asymmetry in the relaxor peak in $\epsilon'(T)$ has been analyzed in terms of the diffuse phase transition model, which describes the temperature dependent dielectric permittivity as well as the size distribution of PNRs by means of a Gaussian function: $\frac{1}{\sqrt{2\pi\sigma^2}} \exp[-\frac{(T-T_m)^2}{2\sigma^2}]$ [26]. Our experimental data can be fitted well by this distribution function and the $\epsilon'(T)$ relaxor behavior was found to be a superposition of three different maxima, denoted as T_m^1, T_m^2, and T_m^3, shown in Fig. 3(a) for $f = 10$ kHz. The experimental data were fitted for all frequencies and three frequency dependent temperatures are presented in Table SM-2 Ref. [32]. Again VF, activation law and power law were tried to fit these three temperatures and we found the Arrhenius behavior provides the best fits as shown in Figs. 3(b), 3(c), and 3(d). The calculated activation energies, 0.22, 0.30, and 0.32 eV, look also physically reasonable. From the deconvolution of the ϵ peaks we obtained three types of PNRs, which may differ in their microscopic origin and have distinguishable size distributions.

These three distinct classes of dipoles can be related to their microscopic origin, taking into account that electric dipoles in TCMO may originate from the oxygen bonds with Co^{2+} and Mn^{4+} ions in the CoO_6 and MnO_6 octahedrons, which are getting distorted/polarized in an applied electric field. The third contribution could be caused by the disorder-induced presence of the Mn^{3+} as well as of Co^{3+} ions. All these PNRs started to interact with lowering temperature. Due to the difference in their distributions as well as in the activation energies they respond differently with external frequency and with temperature. The overall macroscopic response hence, shows a ferroelectric relaxation. Instead of the ferroelectric relaxor-glass-like behavior, described by the VF formalism as a mostly suitable for a dipolar glass model, so our system could be more accurately interpreted by the Arrhenius law. This scenario is an indication that partially disordered TMCO film could be considered as a superparaelectric, i.e., a blocked relaxor at low temperatures and nonzero frequencies, rather than as a dipolar glass.

In order to inspect the mechanisms of interactions among these dipoles, the dielectric loss (ε'') has been analyzed in the frequency domain for different temperatures. For the used frequency range, $f = 20$ Hz–2 MHz, two main mechanisms are known to be responsible for the dipolar relaxation: (1) the Maxwell-Wagner (MW) mechanism originated from the local charge accumulation at grain boundaries [33] and (2) the Debye relaxation, which is the dipolar contribution from the hopping of charge carriers among asymmetric sites (Mn^{4+}, Co^{2+} and Mn^{3+}) [34]. Figure 4(a) shows the dielectric relaxation over the frequency range for the temperatures in the relaxor transition regime. At very low frequencies, $f <$ 200 Hz, one can see a MW behavior, which is manifested by a linear decrease of ϵ with increasing frequency in the logarithmic ω scale. With further increasing frequency the data start to deviate from the MW behavior and display two distinct Debye relaxation peaks at frequencies, denoted as $f_1 = 1/\tau_1$ and $f_2 = 1/\tau_2$. These two relaxation behaviors could be recognized as $\beta(\tau_1)-$ and $\alpha(\tau_2)$-like processes in a glassy system [35]. Indeed, the frequency f_2 increases with increasing temperature and merges with the f_1 at a temperature T_C, which is comparable with the glass transition temperature in an amorphous material [36]. The slower $\alpha(\tau_2)$ relaxation is, analogously to glasses, a primary relaxation process in this dipolar glassy system and can be assigned to the major charge transfer between the Co^{2+}-Mn^{4+} sites. A secondary, or faster β process, develops from the localized disorder or minor sites, occupied likely by Mn^{3+} and/or Co^{3+} ions. Interestingly, one can see that these two processes merge at a temperature around 190 K giving a single relaxation peak at around 100 kHz as shown in Fig. 4(b).

MD analysis has been done by dielectric measurements in an applied magnetic field, $B = 8$ T, at $f = 100$ kHz. Here we can observe a characteristic change in the dielectric constant in the vicinity of the relaxor transition at $T_m \sim 195$ K at this frequency as shown in Fig. 5(a). The temperature dependence of the MD coupling constant $\epsilon_{MD} = \frac{\epsilon'(8T)-\epsilon'(0T)}{\epsilon'(0T)} \times 100$ along with the derivative of dielectric constant ($\frac{\delta\epsilon'}{\delta T}$) in Fig. 5(b) shows that $|\epsilon_{MD}|$ increases by cooling down the system and takes the highest value of 4% close to the relaxor transition.

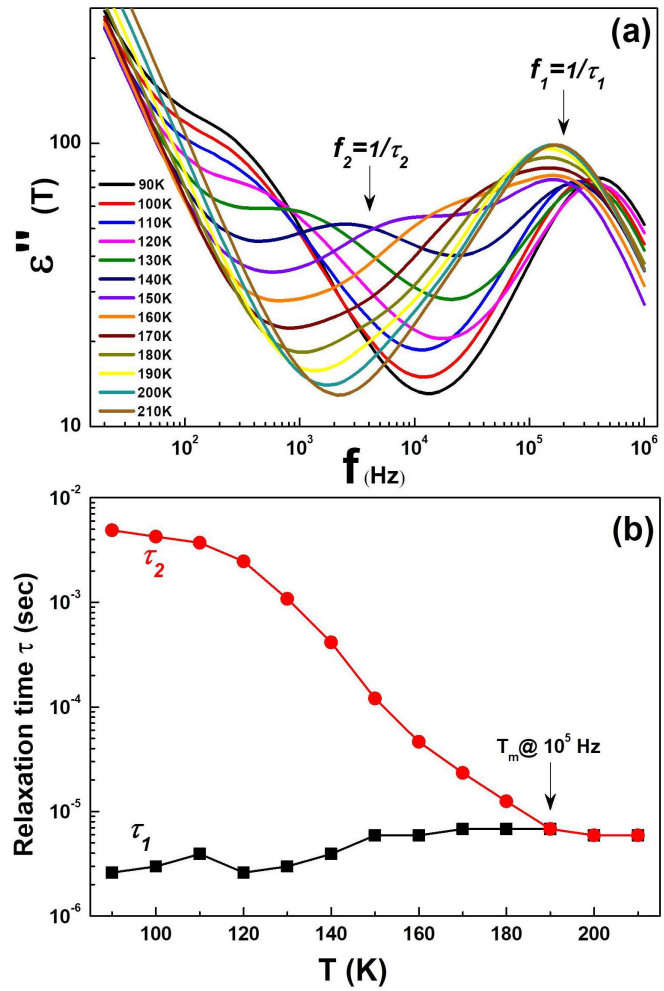

FIG. 4. (a) Frequency dependence of the dielectric loss part $\epsilon''(T)$ measured for different temperatures in the frequency range of $f = 20$ Hz–2 MHz; (b) Temperature dependence of the two different Debye relaxation times $\tau_1 = 1/f_1$ and $\tau_2 = 1/f_2$, evaluated from the positions of peaks in 4(a).

Moreover, the MD effect is negative, i.e., ε' decreases in applied magnetic field. By further lowering the temperature MD coupling decreases again as dipoles are started freezing. The absence of the magnetoresistance [37] (see Fig. SM-3) confirms that the MD coupling is intrinsic to the dipoles present in the material. Moreover, the temperature dependence of electrical resistivity, ρ(T), can be fitted by a variable-range-hopping Mott's behavior [38], $r(T) = r_0 \times \exp(T_0/T)^{1/4}$, with $T_0 = 211$ K and $\rho_0 = 7 \times 10^{-4}\,\Omega$ cm, which illustrates a disorder-dominated charge transport. The so-called Mott temperature $T_0 = 211$ K is given [38] by the formula, $k_B T_0 = b/(g(E_F) \times R^3_{loc})$, where $\beta = 21$ and $g(E_F)$ and R_{loc} are the density of states at the Fermi level and localization radius of charge carriers, respectively. Considering characteristic values of $g(E_F) \sim 10^{27}$–10^{28} $(\text{eV}^*\text{m}^3)^{-1}$ we get $R_{loc} \sim$ 10–5 nm, which is in a good agreement with the nm-scale Co^{3+}/Mn^{3+} disorder in the EELS spectra [24,39] (see Fig. SM-2).

As indicated previously, mostly the Debye processes [35], originating from a charge transfer between dipoles, contribute

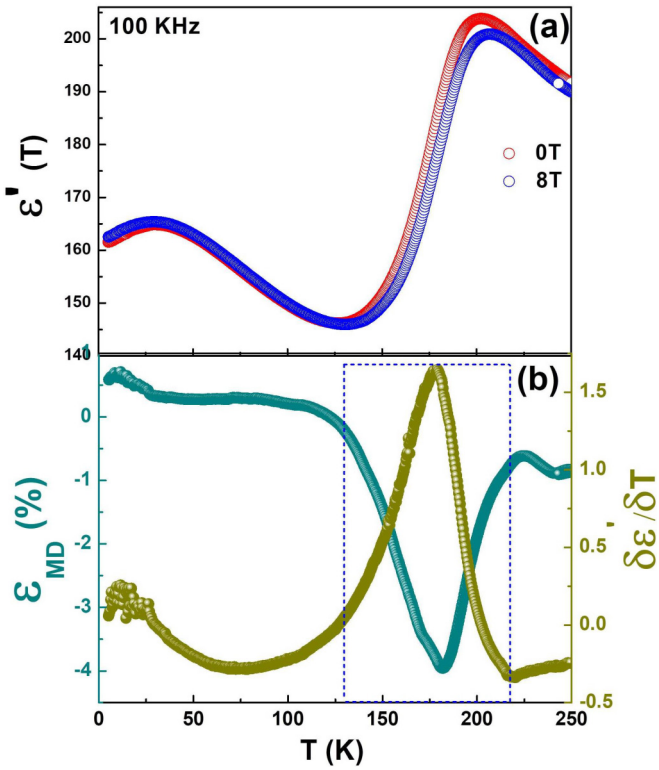

FIG. 5. (a) Temperature dependence of the dielectric constant $\epsilon'(T)$ at 100 KHz without and with applied external magnetic field of 8 T; (b) Temperature dependence of derivative of dielectric constant $(\frac{\delta\epsilon'}{\delta T})$ along with the magneto-dielectric coupling constant ϵ_{MD} (%) showing a maximum 4% magneto-dielectric coupling.

to the dielectric constant at high frequencies. Dielectric constant increases up to the relaxor transition mainly from the contribution of activated dipoles due to the charge transfer from Mn^{3+} to other sites. Below the relaxor transition Mn^{4+} and Co^{2+} start interacting magnetically with the other disorder sites and dielectric relaxation peak splits at the same temperature indicating a charge transfer between them [see Fig. 4(b)]. As the charge transfer is coupled to and depends on the spin arrangement, the short-range spin-spin interaction tries to restrict the charge hopping and we can see the second relaxation peak in Fig. 4 is not that much pronounced as the first one. With applied strong magnetic field this process is further interrupted and dielectric constant further reduce, causing a 4% negative MD coupling at the same temperature.

We have to say that the exact physical mechanism of the observed MD coupling is not known. However, by comparing it with a quite similar high temperature MD effect in the La_2NiMnO_6 [15], a hint into a probable coupling between the disorder-induced local spins in the paramagnetic region and electric dipoles can be given. One can speculate on the coexistence of very similar temperature scales, i.e., for α-β merging around 190 K, for relaxor transition, $T_m \sim 195$ K, and for the resistivity disorder scale $T_0 \sim 211$ K [37] (see Fig. SI-3). Surprisingly, the latter is very close to the charge ordering (CO) temperature in manganites [40,41], i.e., $T_0 \sim T_{CO}$. Note that a peak in a permittivity in THz region was also observed at $T \sim T_{CO}$ in PrCaSrMnO [41]. Likely, the closeness of these temperature scales, where a disorder-induced short range Mn^{3+}/Co^{3+} charge correlations, stabilized at $T < T_0 \sim T_{CO}$, coexist and interplay with superparaelectric dipole regions could result in an unusual MD coupling. It is also highly unexpected to have a spin glass transition at such high temperature that can explain this MD coupling in terms of multiglass behavior. Due to the huge background signal from the substrate and the interface we were unable to resolve any short range spin correlations for $T \gg T_C$ from the Curie-Weis fit of the $1/\chi(T)$ curve. Further detailed studies of the relationship between the B-site disorder and MD coupling are necessary to elucidate its mechanism.

In summary, we have grown monoclinic phase of Tb_2CoMnO_6 double perovskite thin film on Nb : $SrTiO_3$(100) by using the MAD technique. TEM/EELS mapping shows the presence and distribution of both Co^{2+} as well as Co^{3+} ions in the film, evidencing a partial B-site disorder, further confirmed by the observed reduction of the saturation magnetization at low temperatures. The ferromagnetic $T_C = 110$ K was slightly higher as compared to the bulk value due to an in plane tensile strain. Two different dielectric relaxation peaks (β and α) have been observed that merge at a temperature close to the relaxor glass transition. Moreover, we observed an unexpected high temperature relaxor-glass-like transition and a superparaelectric behavior, at which a probable coupling to short range correlated local spin moment results in a 4% magneto-dielectric coupling.

ACKNOWLEDGMENTS

R.M. acknowledges financial support from the Erasmus Plus programme, European Union, Georg-August-Universität Göttingen, and IISER Pune. R.M. and M.C. are grateful to S. Yadav for helping in Dielectric measurement. V.R. and V.M. acknowledge financial support from Deutsche Forschungsgemeinschaft (DFG) via SFB 1073 (TP A02, TP Z02) as well as via DFG Projects No. MO-2254-4 and No. RO-5387/3-1.

[1] Y. Tokura, S. Seki, and N. Nagaosa, Rep. Prog. Phys. **77**, 076501 (2014).
[2] N. A. Spaldin and R. Ramesh, Nat. Mater. **18**, 203 (2019).
[3] M. Bibes and A. Barthélémy, Nat. Mater. **7**, 425 (2008).
[4] M. Coll *et al.*, Appl. Surf. Sci. **482**, 1 (2019).
[5] S. Gariglio, A. D. Caviglia, J. M. Triscone, and M. Gabay, Rep. Prog. Phys. **82**, 012501 (2019).
[6] M. Bibes and A. Barthélémy, IEEE Trans. Electron Devices **54**, 1003 (2007).
[7] L. W. Martin, Y. H. Chu, and R. Ramesh, Mater. Sci. Eng. Rep. **68**, 89 (2010).
[8] M. K. Kim, J. Y. Moon, H. Y. Choi, S. H. Oh, N. Lee, and Y. J. Choi, J. Phys.: Condens. Matter **27**, 426002 (2015).
[9] Y. Shimakawa, M. Azuma, and N. Ichikawa, Materials (Basel) **4**, 153 (2010).
[10] M. Zhu, Y. Lin, E.W.C. Lo, Q. Wang, Z. Zhao, and W. Xie, Appl. Phys. Lett. **100**, 062406 (2012).

[11] C. Meyer, V. Roddatis, P. Ksoll, B. Damaschke, and V. Moshnyaga, Phys. Rev. B **98**, 134433 (2018).
[12] R. I. Dass and J. B. Goodenough, Phys. Rev. B **67**, 014401 (2003).
[13] S. Baidya and T. Saha-Dasgupta, Phys. Rev. B **84**, 035131 (2011).
[14] M. P. Singh, K. D. Truong, and P. Fournier, Appl. Phys. Lett. **91**, 042504 (2007).
[15] D. Choudhury, P. Mandal, R. Mathieu, A. Hazarika, S. Rajan, A. Sundaresan, U. V. Waghmare, R. Knut, O. Karis, P. Nordblad, and D. D. Sarma, Phys. Rev. Lett. **108**, 127201 (2012).
[16] C. Xie, L. Shi, J. Zhao, S. Zhou, Y. Li, and X. Yuan, J. Appl. Phys. **120**, 155302 (2016).
[17] J. Blasco, J. García, G. Subías, J. Stankiewicz, S. Lafuerza, J. A. Rodríguez-Velamazán, C. Ritter, and J. L. García-Muñoz, J. Phys.: Condens. Matter **26**, 386001 (2014).
[18] J. Blasco, J. García, G. Subías, J. Stankiewicz, J.A. Rodríguez-Velamazán, C. Ritter, J. L. García-Muñoz, and F. Fauth, Phys. Rev. B **93**, 214401 (2016).
[19] V. V. Shvartsman, S. Bedanta, P. Borisov, W. Kleemann, A. Tkach, and P. M. Vilarinho, Phys. Rev. Lett. **101**, 165704 (2008).
[20] J. H. Lee, P. Murugavel, H. Ryu, D. Lee, J. Y. Jo, J. W. Kim, H. J. Kim, K. H. Kim, Y. Jo, M. H. Jung, Y. H. Oh, Y. W. Kim, J. G. Yoon, J. S. Chung, and T. W. Noh, Adv. Mater. **18**, 3125 (2006).
[21] M. Jungbauer, S. Hühn, R. Egoavil, H. Tan, J. Verbeeck, G. Van Tendeloo, and V. Moshnyaga, Appl. Phys. Lett. **105**, 251603 (2014).
[22] J. Y. Moon, M. K. Kim, D. G. Oh, J. H. Kim, H. J. Shin, Y. J. Choi, and N. Lee, Phys. Rev. B **98**, 174424 (2018).
[23] See Supplemental Material at http://link.aps.org/supplemental/10.1103/PhysRevB.101.094426 for x-ray diffraction pattern.
[24] See Supplemental Material at http://link.aps.org/supplemental/10.1103/PhysRevB.101.094426 for TEM and EELS.
[25] M. Tyunina and J. Levoska, Phys. Rev. B **70**, 132105 (2004); See Supplemental Material at http://link.aps.org/supplemental/10.1103/PhysRevB.101.094426 for fitting parameters of the Curie-Weiss law (Table S1-1).
[26] C. W. Ahn, C. H. Hong, B. Y. Choi, H. P. Kim, H. S. Han, Y. Hwang, W. Jo, K. Wang, J. F. Li, J. S. Lee, and I. W. Kim, J. Korean Phys. Soc. **68**, 1481 (2016).
[27] A. A. Bokov and Z. G. Ye, Front. Ferroelectr. A Spec. Issue J. Mater. Sci. **1**, 31 (2007).
[28] D. Viehland, S. J. Jang, L. E. Cross, and M. Wuttig, J. Appl. Phys. **68**, 2916 (1990).
[29] A. E. Glazounov and A. K. Tagantsev, Appl. Phys. Lett. **73**, 856 (1998).
[30] L. Eric Cross, Ferroelectrics **76**, 241 (1987).
[31] A. R. von Hippel, *Dielectrics, and Waves* (MIT Press, Cambridge, MA, 1966).
[32] See Supplemental Material at http://link.aps.org/supplemental/10.1103/PhysRevB.101.094426 for fitted peak temperatures in frequency and temperature dependent permittivity.
[33] K. C. Kao, *Dielectric Phenomena in Solids* (Elsevier Academic Press, London, 2004).
[34] F. Kremer and A. Schönhals, *Broadband Dielectric Spectroscopy* (Springer-Verlag, Berlin, Heidelberg, 2003).
[35] P. Lunkenheimer, U. Schneider, R. Brand, and A. Loidl, Contemp. Phys. **41**, 15 (2000).
[36] H. B. Yu, W. H. Wang, H. Y. Bai, and K. Samwer, Natl. Sci. Rev. **1**, 429 (2014).
[37] See Supplemental Material at http://link.aps.org/supplemental/10.1103/PhysRevB.101.094426 for resistivity vs temperature behavior measured for ambient ($B = 0$) and applied magnetic field $B = 8$ T.
[38] N. F. Mott, Conduction in non-crystalline materials, Philos. Mag. **19**, 835 (1969).
[39] R. Egoavil, S. Hühn, M. Jungbauer, N. Gauquelin, A. Béché, G. Van Tendeloo, J. Verbeeck, and V. Moshnyaga, Nanoscale **7**, 9835 (2015).
[40] M. Uehara, S. Mori, C.H. Chen, and S.-W. Cheong, Nature (London) **399**, 560 (1999).
[41] A. Pimenov, M. Biberacher, D. Ivannikov, A. Loidl, A. A. Mukhin, Yu. G. Goncharov, and A. M. Balbashov, Phys. Rev. B **73**, 220407(R) (2006).

Correction: A DFG Project Number in the Acknowledgment section contained an error and has been fixed.